Composite Structures 297 (2022) 115922

Contents lists available at ScienceDirect

Composite Structures

journal homepage: www.elsevier.com/locate/compstruct

Effect of voids on the impact properties of Non-Crimp fabric carbon/epoxy laminates manufactured by liquid composite Moulding

Julen Mendikute *, Maider Baskaran, Laurentzi Aretxabaleta, Jon Aurrekoetxea

Mechanical and Industrial Production Department, Mondragon Unibertsitatea, Loramendi 4, 20500 Arrasate-Mondragón, Spain

ARTICLE INFO

Keywords:
Liquid Composite Moulding
Void content
Impact properties

ABSTRACT

A great effort has been made to quantify the detrimental effect of voids on CFRP, nevertheless, the effect on impact properties has been barely studied and when it has been considered, it has always been for prepeg materials and under low impact energies (< 6 J). This work focuses on the quantification of the effect of voids on the impact properties of NCF plates manufactured by LCM. For this purpose, biaxial (0/90) NCF-Epoxy laminates with different void contents were tested by the drop weight impact method. Four LCM variants were used to obtain plates at different void levels: VARTM with controlled modified capillary number (0.58 ± 0.18 %), RTM with controlled modified capillary number (1.35 ± 0.28 %), uncontrolled RTM (2.44 ± 0.14 %), and WCM (4.34 ± 0.31 %). The high void content samples (WCM) recorded a reduction of 25.88% in ultimate fibre failure force F_{ff}, and 9.57% in dissipated energy E_{dis} as compared to the low void content samples (VARTM-Ca_{opt}*). Regarding the analysis of damage tolerance, the loss of stiffness after impacts ranging from 2.5 J to 20 J was studied. A slightly higher loss was observed in WCM plates compared to VARTM-Ca_{opt}*, the residual stiffness after 20 J impacts being 45.8% and 49.1%, respectively. Therefore, to achieve optimum impact properties it is necessity to develop controlled LCM manufacturing processes that approach zero-defect manufacturing.

1. Introduction

Carbon Fibre Reinforced Polymers (CFRP) have emerged as a promising material for structural applications where lightweighting is a key factor. CFRP combine low density with good mechanical properties, such as high specific strength and stiffness, toughness, and good corrosion resistance [1]. Among the different CFRP textile architectures, unidirectional (UD) has been widely used in industry [2]. However, the properties are high only in the fibre direction and not in the transversal direction [3]. Two-dimensional (2D) woven textiles improve the properties in the transversal direction, but adversely the longitudinal properties are reduced due to the waviness of the fibres. For this reason, recent studies have focused on the development of Non-Crimp Fabrics (NCF), which are composed of multiple UD layers stitched together and which provide high in-plane properties [4,5].

Despite CFRP potential, the lack of automation in the manufacturing process (autoclave-based) means the cost of producing CFRP is prohibitive, which has hindered the mass usage of these materials in the automotive industry [6]. In an attempt to reduce operational costs, Liquid Composite Moulding (LCM) technologies, and in particular Resin Transfer Moulding (RTM) and Wet Compression Moulding (WCM) have been employed. Nonetheless, LCM processes do not achieve the quality standards of the robust autoclave process, mainly due to process-induced void defects [7]. While voids can be caused by a variety of factors, mechanical air entrapment is thought to be the most common cause of void creation in LCM [8]. Therefore, understanding void minimisation strategies and quantifying the effect of voids on mechanical performance is essential to manufacture zero-defect parts and achieve the robustness required by the industry [9].

Unlike single-scale fabrics (random mats), dual-scale fabrics that group fibres in tows (NCF and weave textiles), are filled with a two-level impregnation mechanism which is susceptible to generating voids [10]. At low impregnation velocities, the capillary effect is severe, making the velocity inside the tows faster than outside. This leads to the generation of macro-voids between the tows. Nevertheless, at high impregnation velocity, the viscous force predominates and makes the velocity outside the tows faster, generating micro-voids inside the tows. The balance of both, viscous and capillary forces, is quantified by the modified capillary number (Ca^*) proposed by Patel et al. [11]. When these forces are balanced, the intra-tow and inter-tow impregnation is compensated, and

* Corresponding author.
E-mail address: jmendicute@mondragon.edu (J. Mendikute).

https://doi.org/10.1016/j.compstruct.2022.115922
Received 15 September 2021; Received in revised form 25 May 2022; Accepted 18 June 2022
Available online 23 June 2022

the generation of voids is reduced. This means that for each fabric-matrix system there is an optimal modified capillary number (Ca_{opt}*), and hence, an optimal impregnation velocity (υ_{opt}). A promising technique that uses the Ca_{opt}* to reduce void content is that proposed by Trochu et al. [12], and implemented by Ruiz et al. [13]. They proved that an adaptive injection system controlled the flow-front velocity at every instant to ensure a Ca_{opt}*, and thus minimum void content was achieved in the entire part. This solution stands out from approaches such as bleeding or consolidation, which are expensive and difficult to apply to complex geometries [14].

Many papers can be found in the literature demonstrating the importance of void reduction, and analysing the effect of void content on different mechanical properties. The consensus in the literature is that matrix-dominated properties are clearly affected by the void content, whereas in the fibre-dominated properties the effect is not so evident [8]. The majority of these studies are related to prepreg textiles, where voids are generated by modifying the consolidation pressure [15]. There are few works available about the effect of voids on the reduction of mechanical properties of NCF manufactured with LCM. To date, the detrimental effect of voids in NCF-LCM composites has been demonstrated in the following matrix-dominated properties: compression modulus and strength [16], flexural modulus and strength [17], fatigue strength [18–20], and inter-laminar fracture toughness [21]. Conversely, a minor or negligible reduction has been observed in the fibre-dominated properties such as longitudinal tensile modulus and strength [18]. Likewise, it is proved that voids have greater effects on the reduction of out-of-plane properties than in-plane properties [22].

The effect of voids on out-of-plane impacts has been studied only at low-energy impacts: less than 1 J [23,24] and less than 6 J [25]. The results were not entirely conclusive since they showed that the voids could facilitate the initiation and propagation of crack, but at the same time could stop propagation due to plastification of the matrix. One of the limitations of these studies is that they were focused at very low impact energies. In addition, all reviewed studies used prepeg composites where voids (mostly intra-laminar) were generated by curing cycle modification. No studies have been found about the effect of voids on out-of-plane impacts in NCF-LCM composites.

This paper presents a study on the effect of voids on out-of-plane impacts (drop weight impact test) of CF-Epoxy NCF laminates manufactured with LCM. For this purpose, a practical methodology similar to the one used by Leclerc and Ruiz [26] was followed. The mechanism of void formation in LCM variants was studied to find the method that minimizes the formation of voids. In this way, it was possible to manufacture plates with different void levels. These plates were used to study the impact performance by means of ultimate fibre failure force (F_{ff}) and dissipated energy (E_{dis}) for both subcritical and supercritical impacts. Finally, the effect of voids on damage tolerance was investigated.

2. Materials and experimental methods

2.1. Materials

Symmetric Laminates composed of four plies of a biaxial (0/90) NCF of 50 k high resistance carbon fibre compacted to 3 mm (reference HPT 610 C090 from SGL) were used in this study. The fibre density and the preform areal weight provided by the manufacturer were 1750 kg/m^3 and 610 g/m^2, respectively. An epoxy binder powder (Araldite LT 3366 BD) was added, 15 g/m^2 per layer, to maintain the integrity of the preform during cutting, handling and injection. The binder reduced the fraying of the edges during the cutting and handling of the preform, and consequently the risk of race-tracking on the preform edges was greatly reduced. Moreover, the binder kept the net-shaped preform compacted and prevented slippage between the layers during injection [27].

The resin used was a fast curing epoxy resin (Araldite® XB 3585) and hardener (Aradur® 3475) supplied by Huntsman. The density of the mixture was 1161 kg/m^3, and the mixture ratio was 100:21 in weight.

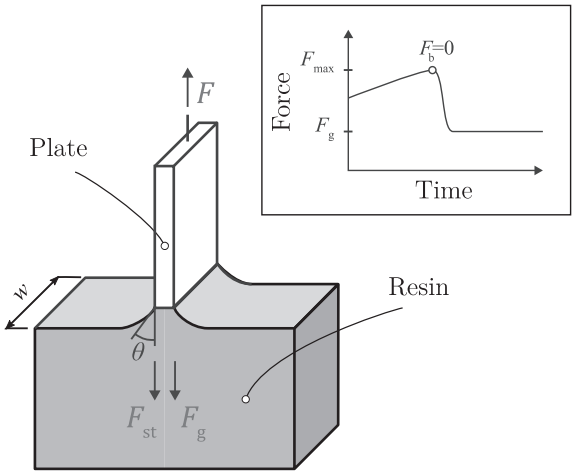

Fig. 1. Wilhelmy method: instant prior to the total emersion of the plate (F_b = 0).

2.2. Physical properties: Density, fibre volume fraction, and void content

The density of the composite samples, ρ_c, was determined in accordance with the liquid displacement method (ASTM D 792). This method is based on Archimedes principle, which measures density by weighing the sample in air and immersed in distilled water. Ohaus Galaxy™ 110 (1 mg accuracy) balance was used for the fibre (ρ_f), matrix (ρ_m), and composite sample (ρ_c) measurements.

The burn-off method described in ASTM D3171 was used to determine the fibre volume fraction (υ_f) and the void fraction (υ_v) of the samples by burning the samples for 5 h at 500 °C in a muffle. Bodaghi et al. [28] carried out thermogravimetric measurements to confirm that carbon fibre is stable in the range of 300–500 °C and degrades beyond 900 °C. This way, they demonstrated the suitability of the burn-off method for void content and fibre volume determination in CFRP. Weighing the sample before (w_c) and after the burn-off (w_f), the results of fibre volume fraction and void volume fraction were obtained:

$$v_f = \frac{w_f \rho_c}{w_c \rho_f} \tag{1}$$

$$v_v = 1 - \left(v_f + \frac{(w_c - w_f)\rho_c}{w_c \rho_m} \right) \tag{2}$$

2.3. Specimen fabrication

As mentioned in the introduction, each resin-fabric system has an optimum modified capillary number, Ca_{opt}*, and is calculated by the following equation:

$$Ca^*_{opt} = \frac{\mu v_{opt}}{\gamma \cos\theta} \tag{3}$$

where μ is the viscosity of the resin, v_{opt} is the optimum velocity of the flow front, γ is the surface tension of the resin, and θ is the resin-fibre contact angle. In order to obtain the Ca_{opt}* that ensures the lower void content, these parameters were characterized using the methods described below.

For the determination of the resin viscosity, a Brookfield viscometer was used (PCE-RVI 2 with L2 type spindle). A stirrer placed in the liquid resin measures the increasing torsional resistance of the fluid due to the curing of the resin. However, the high reactivity of the resin at high temperatures made it difficult to determine the Ca*, as the viscosity increased exponentially over time. Therefore, the resin viscosity was analysed at low temperatures (less than40 °C), where it hardly changed

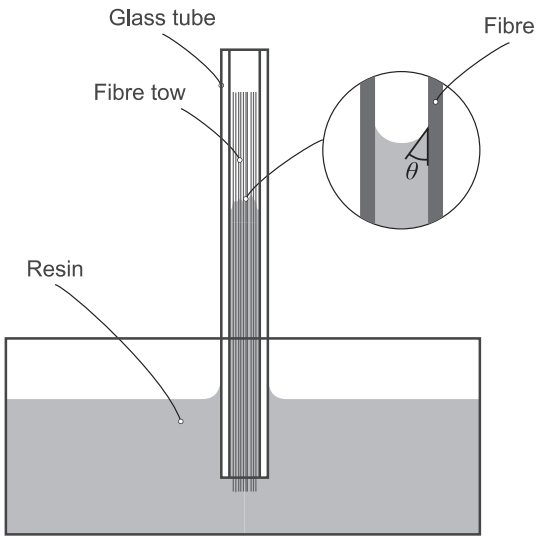

Fig. 2. Wicking test fixture used for posterior contact angle detection in XCT [30].

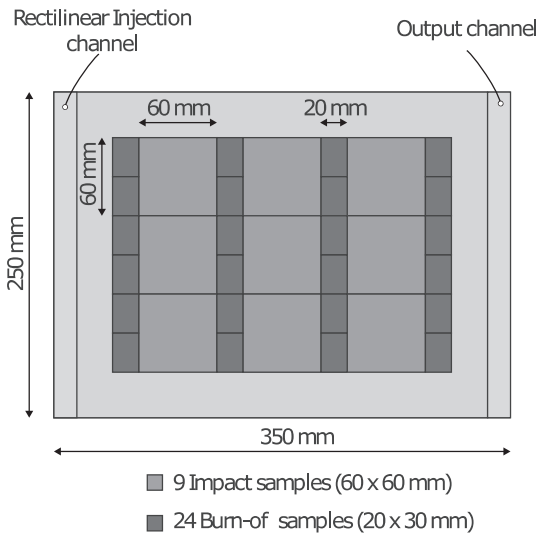

Fig. 3. Position of specimens throughout the resin flow for later evaluation of void content and impact testing.

over the duration of the tests.

Wilhelmy plate method was used for the surface tension measurement and it was done in the Textechno Favimat machine [29]. In this method a thin plate is immersed in the analysed liquid. The plate is pulled up at a slow rate (1 mm/min), and the force on the plate is measured by a tensiometer. While the plate is immersed in the fluid, gravity force (F_g), buoyancy force (F_b), and surface tension (F_{st}) are acting on the plate. At the last instant before the plate completely emerges from the liquid (Fig. 1), the buoyancy force decreases to zero. At the last instant of contact between the plate and the liquid, the force is maximum (F_{max}), and is the sum of the gravitational force (F_g) and the surface tension (F_{st}):

$$F_{max} = F_g + F_{st} = mg + 2w\gamma\cos(\theta) \tag{4}$$

where g is the gravitational constant. It is important to mention that the perimeter of the plate was considered 2w, where the perimeter of the thickness was considered negligible. When the plates emerges from the liquid, F_g is the only acting force. Taking the force drop (F_{max}-F_g), and assuming that the contact angle between the plate and the liquid (θ) is zero due to the complete wetting, the surface tension (γ) can be calculated as follows:

$$\gamma = \frac{F_{max} - F_g}{2w} \tag{5}$$

where w is the width of the plate. The original Wilhelmy method used a platinum plate, because it can be completely wetted due to its high surface free energy, and thus the contact angle between the plate and the liquid can be considered zero. However, paper filters were used, as they are also effective but much cheaper and more accessible [30]. To ensure that the surface tension is invariable over time, different measurements were taken at different curing times (2 min, 6 min, 12 min, 24 min, 36 min, and 48 min).

The contact angle between the resin and the fibre was measured by X-ray micro-computed tomography (XCT) (Phoenix Nanotom 160 kV) [30]. For this purpose, a single carbon fibre tow was placed in a vertical borosilicate glass tube of 0.8 mm diameter and 95 mm height. This tube was placed in a cubic tank containing liquid resin (Fig. 2). The capillary forces caused the resin to rise and impregnate the carbon fibre tow. The resin was then cured at room temperature for 24 h. The XCT scanning produced a 3D volume containing 2304 transverse slices with 1180 × 1180 pixels. Several meniscus images were detected, which were processed by means of a Python® code for the segmentation of the air, resin and fibre phases. The contact angle between the fibre and resin was calculated by fitting the meniscus parabola and the fibre line (detail in Fig. 2).

The last step in obtaining the Ca_{opt}* was the determination of the void content as a function of the impregnation velocity. A strategy of constant pressure injection cannot ensure a constant impregnation velocity during the filling, since the flow-front position increases and thus the pressure gradient and the impregnation velocity are reduced over time. For that reason, in order to obtain an invariable impregnation velocity, a controlled flow-rate injection strategy was chosen [31]. The theoretical impregnation velocity for a given injection flow-rate (Q_{inj}), mould cavity thickness (h), mould length (y), and porosity (ϕ) is calculated according to the following equation:

$$v_{ff} = \frac{Q_{inj}}{\phi h y} \tag{6}$$

A stainless steel mould was used to manufacture composite plates (Fig. 3). It was mounted in a hydraulic press (Hidrogarne MV-80) and the plate dimensions were 350 mm × 250 mm with a thickness of 3 mm. The temperature of the mould was controlled with a hydraulic heater system (Regloplas 300 s). The temperature was chosen based on viscosity measurements to ensure a filling time shorter than the gel time. The injection point was connected to the electric injection system (2100 cc Series RTM RADIUS Injection System), which controlled the resin injection with a constant flow rate. It was important to maintain an area without textile (injection channel) at the beginning in order to accomplish a rectilinear injection. As a result, when the resin was injected into the mould, it filled the whole channel before impregnating the textile, resulting in a homogenous rectilinear injection. From each plate, nine 60 mm × 60 mm specimens were obtained for impact tests, and 24 specimens of 30 mm × 20 mm were obtained for void content quantification by burn-off.

After determining the void content as a function of the impregnation rate, equation (3) was used to calculate the void content as a function of the capillary number. It was possible to determine the capillary number

Table 1
Strategies used for the manufacture of the CF-Epoxy plates.

Name	Process	Ca_{opt}*	Vent
$VARTM_{opt}$	RTM	✓	✓
RTM_{opt}	RTM	✓	×
RTM	RTM	×	×
WCM	WCM	×	×

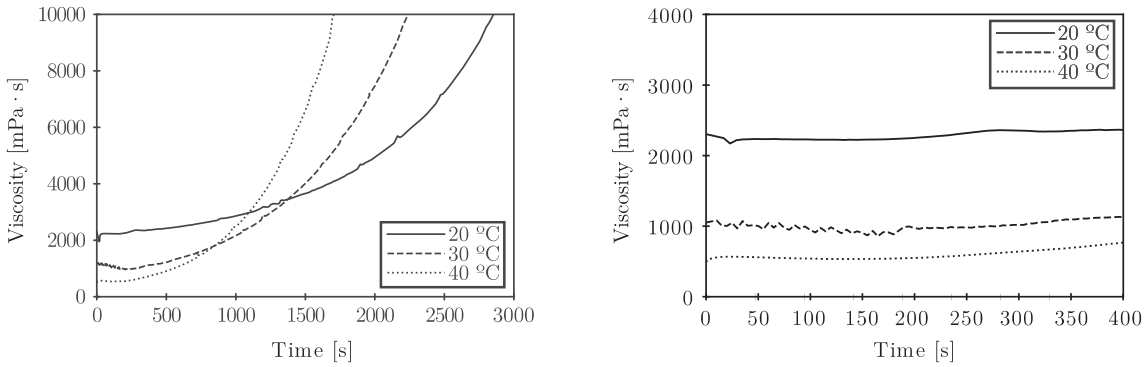

Fig. 4. Resin viscosity evolution for 20 °C, 30 °C, and 40 °C in 3000 s, and b) in 450 s.

since all the components of the equation were characterised; the viscosity, the impregnation velocity (which generates different levels of voids), the contact angle, and the surface tension. To select the manufacturing conditions, the original intention was to choose four levels of capillary number that would generate four levels of void content. However, it was not possible to obtain plates with void content lower than 1% or higher than 3%. Therefore, the four levels of voids that were compared were manufactured as explained in Table 1. The first type of plate ($VARTM_{opt}$) was manufactured with Vacuum Assisted RTM, and the flow front velocity was controlled to ensure the Ca_{opt}* during the injection. The second case (RTM_{opt}) was similar to the previous case, optimum injection was applied, but without applying the vent for the evacuation of voids. The third case (RTM) was also manufactured using RTM, but in this case non-optimal injection parameters were used, i.e., the flow front velocity was not adjusted to the optimum velocity and no vacuum was applied at the outlet. In the last case Wet Compression Moulding (WCM) was used, since the void content is generally around 4–5% [32]. A summary of the four techniques used can be found in Table 1. To obtain a reliable result, at least three plates of each type were produced.

2.4. Drop weight impact test

Initially, for the experimental campaign, three plates were produced for each void level, so 27 samples (60 mm × 60 mm) per void level were fabricated. These samples were tested at nine different impact energies (1 J, 4 J, 8 J, 20 J, 30 J, 40 J, 50 J, 60 J, and 70 J) and three repetitions per energy. However, in the subsequent analysis of the results, it was found convenient to analyse three new energies (2.5 J, 12.5 J, and 55 J). For this purpose, another plate was made for the case of the lowest and highest void content.

Low velocity impact tests were carried out at room temperature with a drop weight impact machine (Fractovis-Plus Ceast), where impact energy is defined by setting the impactor mass and height. For impacts below 20 J a mass of 2.045 kg was used and the height was the parameter to be varied from 0.05 m (1 J) to 0.995 m (20 J). In the case of impacts above 20 J, a mass of 7.25 kg was used, and the height was changed again up to 70 J. The sample was clamped with a circular ring of outer and inner diameter of 60 mm and 40 mm, respectively. In addition, the testing machine was equipped with an anti-rebound system to avoid multiple collisions that could alter the results. A hemispherical metallic striker with a diameter of 20 mm was used, and it was equipped with a 20 kN cell load that enabled to record the force–time $F(t)$ data during the impact. From the $F(t)$ curve, the dissipated energy, $E(t)$ and the displacement of the sample, δ(t) were calculated using the following equations:

$$\delta(t) = \delta_i + v_i t + \frac{gt^2}{2} + \int_0^t \left(\int_0^t \left(\frac{F(t)}{m} \right) \mathrm{d}t \right) \mathrm{d}t \tag{7}$$

$$E(t) = m\left(V_i^2 - V^2(t)\right) + mg\delta \tag{8}$$

where δ_t and δ_i are the displacement at time t and initial displacement, v_i is the initial velocity of the impactor, g is the gravitational acceleration, $F(t)$ is the force at time t, and m is the impactor mass.

The delamination threshold energy (E_d), was used to classify the impacts as supercritical or subcritical based on whether the incident energy was above or below the threshold (E_d), respectively.

For the characterisation of the residual stiffness curve, the three-test characterisation method defined by Feraboli and Kedward [33] was followed. The samples were subjected to subcritical impacts (1 J) before and after the damage-inducing impact. The contact time ratios of subcritical impacts were used to obtain the relative residual stiffness curve equivalent to the normalised compression after impact [34].

2.5. Optical microscopy and impact damage inspection

The microstructure of the cross section of the part was analysed by means of an optical microscope (Leica DM300). A 20-magnification lens was used and a scanning was performed along the section. In order to analyse the samples under the microscope, they were first cut on a metallographic saw using an abrasive disc. Afterwards, an initial polishing with silicon carbide abrasive paper and final polishing with a synthetic diamond compound on the inspection face were performed.

Non-destructive ultrasonic inspections were performed on each impacted specimen in order to determine the shape and area of post-impact delamination. The equipment used consists of an OmniScan MXU portable flaw detector, two-axis GLIDER™ scanner, broadband phase array probe of 5 MHz and specific wedges. By using a Python® image processing code, it was possible to quantify the delaminated area in each sample.

3. Experimental results and discussion

3.1. Specimen fabrication

To define the injection conditions, the first step was to characterise the viscosity of the resin and to choose the injection temperature. The following two injection criteria, among others, had to be met: 1) the injection time had to be shorter than the gel time (in order to ensure complete impregnation) and 2) the viscosity of the resin had to remain relatively constant during injection. The second criterion was established in order to control the Ca*. By keeping the viscosity constant and controlling the impregnation velocity, it was possible to produce plates of constant Ca*. As the resin is highly reactive, its viscosity was characterised at low temperatures (20 °C, 30 °C, 40 °C) (Fig. 4.a). In addition, its evolution was analysed in the first 450 s, which was sufficient for manufacturing the plates. Fig. 4.b shows that the variability of the viscosity is quite low in that time window, 2.79% for 20 °C, 7.75% for

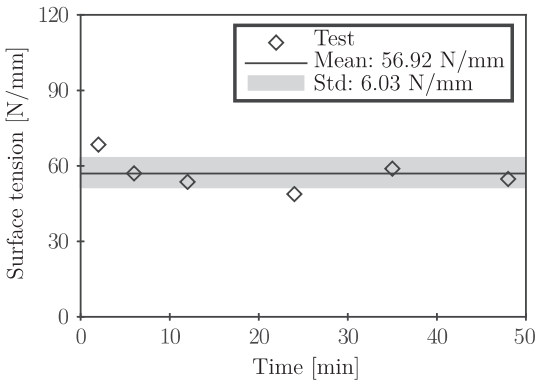

Fig. 5. Surface tension evolution over time.

30 °C, and 14.19% for 40 °C. Therefore, the temperature chosen for the manufacturing the plates was 40 °C, with a viscosity of 613 ± 87 mPa·s, as it was observed that the viscosity remained relatively constant up to 400 s. In this time range, its viscosity increased from 615 °C to 692 °C, being an increase of 12.5%.

The surface tension measurements showed no variation over time and a value of 56.92 ± 6.03 N/mm was obtained (Fig. 5).

For the calculation of the contact angle, rendered XCT volumes were scanned and nine fibre-resin menisci were obtained (Fig. 6). An image-processing algorithm developed in Python® was used to calculate the contact angle, which resulted in a value of 47.80 ± 3.52°.

Finally, plates were produced at different injection rates, and by means of the Ca^* equation (Eq. (3)) it was possible to relate the void levels and Ca^* numbers (Fig. 7). The high reactivity of the resin did not allow a value of Ca^* of less than 0.02, since a reduction of the injection velocity or viscosity (by increasing temperature) resulted in premature curing without total impregnation of the part. In addition, it was not possible to produce plates with a Ca^* higher than 0.14, as increasing the viscosity or the injection velocity resulted in excessive internal pressure giving rise to textile deformation (washout) [35]. It can be seen that between Ca^*=0.02 and Ca^*=0.14 there is a range around Ca^*=0.09 where the void content is the minimum but not less than 1%.

To obtain plates with a void content of less than 1%, plates with Ca^*_{opt} were manufactured, and vacuum was applied at the mould outlet. On the other hand, to manufacture plates with a void content higher than 4%, WCM was used. The results of the physical properties of fibre content, matrix and voids of the four types of fabricated plates are shown in Table 2. It can be observed that the plates manufactured with RTM and following the criteria of Ca^*_{opt} ($VARTM_{opt}$) where vacuum was also applied, resulted in a void content lower than 1% (0.58 ± 0.18%). This result was in good agreement with the previous findings of Lebel et al. [36], who achieved plates with void content lower than 1% by searching for the optimum capillary number. In the case of the plates with the Ca^*_{opt}, but without vacuum (RTM_{opt}), the void content was 1.35 ± 0.28%. When RTM with non-optimal conditions was used, the void content obtained was 2.44 ± 0.14%. Plates manufactured with WCM showed a higher level of voids, even exceeding 4% (4.34 ± 0.31%). Lee et al. [32] obtained similar void content (4.9%) for CF-Epoxy NCF manufactured with WCM. Fig. 8 shows in detail the qualitative difference in void content between the $VARTM_{opt}$ and WCM samples.

3.2. Drop weight impact test

3.2.1. Single impact

For the classification of the energy regimes, the damage threshold

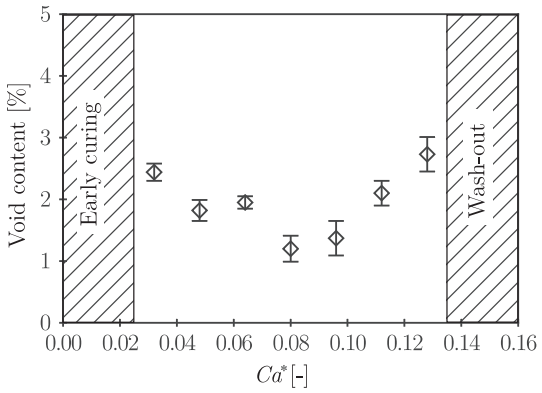

Fig. 7. Void content for different Ca^* (within processability limits) with lower void content at Ca^*=0.09.

Table 2
Void content and fibre volume for the four types of plates.

	Fibre volume [%]	Void content [%]
$VARTM_{opt}$	46.18 ± 0.91	0.58 ± 0.18
RTM_{opt}	46.53 ± 0.92	1.35 ± 0.28
RTM_{opt}	45.85 ± 0.80	2.44 ± 0.14
WCM	46.27 ± 1.36	4.34 ± 0.31

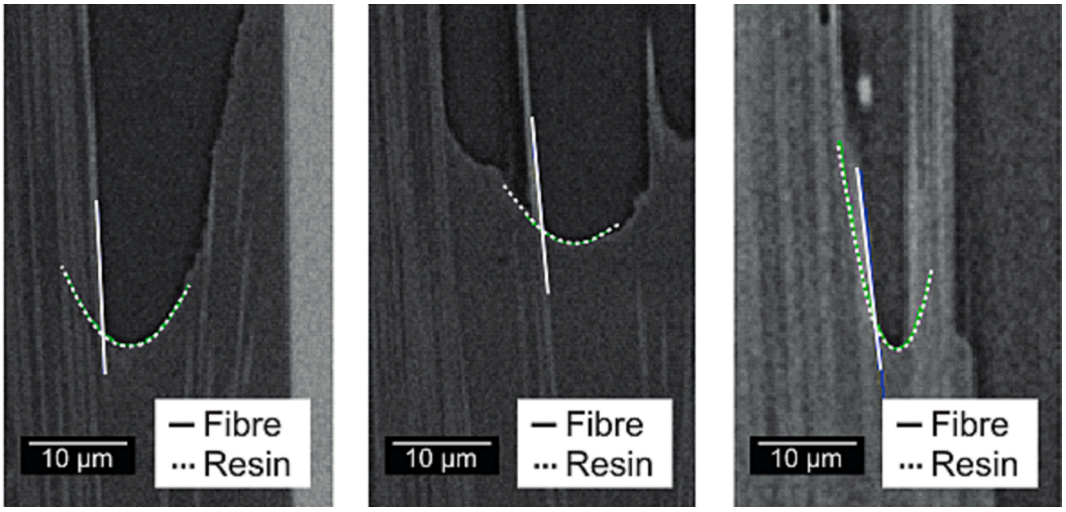

Fig. 6. Calculation of the contact angle using images from XCT.

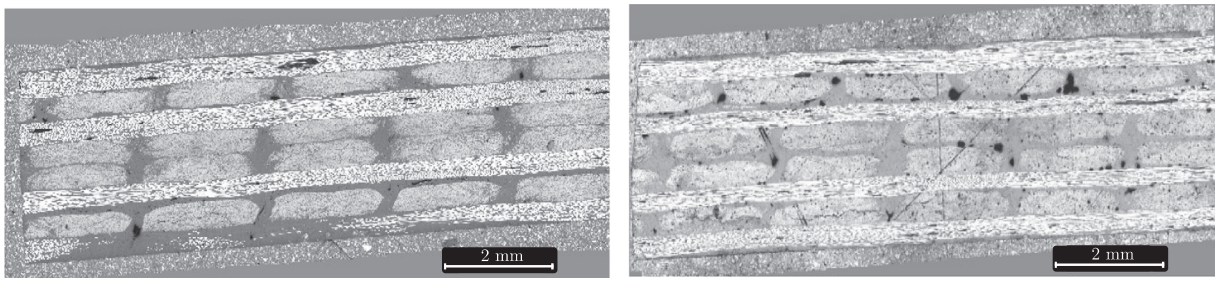

Fig. 8. Microscope images for the detection of voids for a) VARTM$_{Ca^*}$ and b) WCM.

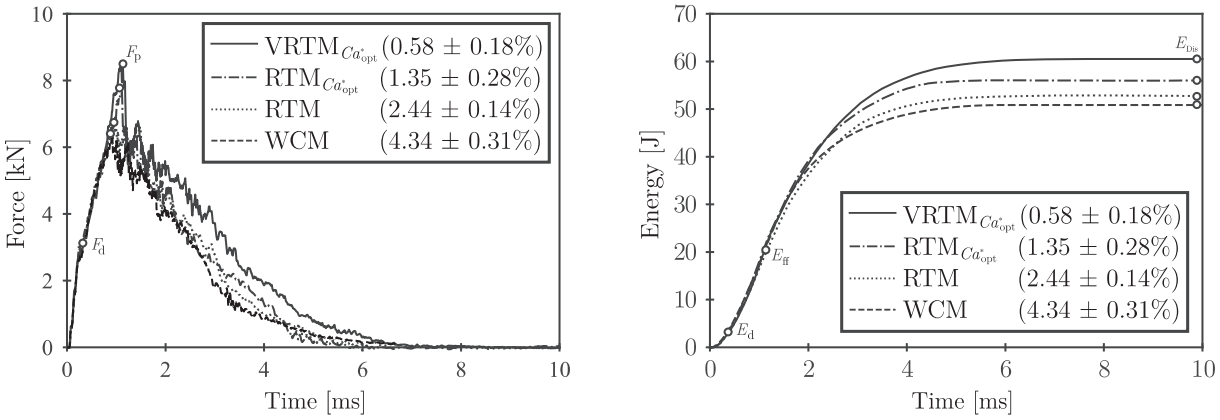

Fig. 9. Evolution of force and energy over time for 70 J supercritical impacts on VARTM$_{Ca^*}$ plates.

(delamination threshold) was first determined by 70 J impacts (Fig. 9). The delamination energy, E_d, at which the damage initiated, was identified by the force F_d which caused a reduction in stiffness [34,37]. Impact energies below E_d were labelled as subcritical impacts, and those above E_d as supercritical impacts. The E_d was similar for all void contents, and had a value of 1.5 J ± 0.1 J. The ultimate fibre failure force (F_{ff}) gives information on the onset of fibre breakage, and the energy threshold of fibre breakage E_{ff}, could be determined being 19.8 J ± 0.3 J for all four types of plates. Thus, supercritical impacts were classified into supercritical inducing delamination (Supercritical I) and supercritical inducing fibre rupture (Supercritical II).

To validate the classification of energy ranges, a fractographic analysis was carried out on samples impacted with three diferent energies 8 J, 20 J and 70 J. In the 8 J impact it was showed that once the E_d threshold is exceeded (1.5 J) some delamination and matrix cracks appeared (Fig. 10a). In this range of energies lower than E_{ff} there was not fibre failure. However, when impact energy was higher than E_{ff} fibre failure was detected in addition to delamination and matrix breakage, as showed in samples impacted with 20 J (Fig. 10b). Therefore, it can be confirmed that at energies slightly below 20 J fibre failure occurs, coinciding with the E_{ff} detected in the 70 J impacts (19.8 J). Finally, a specimen impacted at 70 J is showed (Fig. 10c), where it can be seen that all the failure modes mentioned above are present. In addition, the part was not able to maintain its structural integrity and the impactor perforated the entire sample.

The F_p and the dissipated energy (E_{Dis}) was different for each of the plates. Fig. 11 shows the F_p (Fig. 11.a) and E_{dis} (Fig. 11.b) obtained for the four types of fabricated plates. The reduction of both properties can be observed for an increase in void volume. The F_p was reduced by as much as 25.88% for void contents between 4 and 5% frequently obtained in WCM. On the other hand, in the case of energy dissipation, the plates with high void content (WCM) dissipated 9.57% less energy.

For clarity, in the subsequent analysis only the values of the two extremes of void content are shown, i.e., VARTM$_{opt}$ (0.58 ± 0.18%) and WCM (4.34 ± 0.31%). The samples were subjected to several single impacts from which the F_p recorded in each of the tests was extracted. Fig. 12 shows the same F_p for the samples with low void content (VARTM$_{opt}$) versus the samples with high void content (WCM). The results obtained with samples RTM$_{opt}$ and RTM have been omitted. It can be seen that both samples followed the same trend, however the values for the high void content samples were slightly lower. The graph shows how below E_{ff} the maximum force increases with the impact energy. Furthermore, it can be seen how the VARTM$_{opt}$ values are slightly higher than WCM. At E_{ff} (which is the similar for both samples), the F_p reaches a plateau at 8,411 ± 387 N and 6,423 ± 206 N for low and high void content, respectively.

Fig. 13 plots the evolution of the dissipated energy (E_{dis}) versus the impact energy (E_0). The dashed line represents the limit where E_{dis} is equal to E_0, which is physically impossible to exceed. Above 50–55 J, perforation threshold, the specimen is perforated and the dissipated energy remains constant. However, the maximum dissipated energy is lower for WCM 51.5 ± 1.3 J compared to 56.1 ± 1.1 J for VARTM$_{opt}$.

The recorded force–time curves for subcritical impacts (1 J) revealed a different behaviour for the low and high void content samples (Fig. 14). In both cases, the asymmetric curve is a clear example of energy loss even at subcritical energies [38]. Firstly, the contact time between the impactor and the specimen was slightly different: A contact time of 2.54 ± 0.06 ms and 3.08 ms ± 0.11 ms was recorded for the low and high void content plates, respectively. This represents a 20% increase in contact time of high void content samples. In the same way, at low void contents, the peak force was 35% higher: 2,676 ± 452 N to 1,985 ± 219 N. This difference is higher than that detected in the supercritical impacts, where the difference in peak force between the low and high void content samples was 25.9%.

In order to quantify the difference in bending stiffness, the force–displacement curve of both samples were analysed (Fig. 15). The displacement is obtained by integrating the force as described in equation (7). The force increased linearly to a maximum (load phase), and

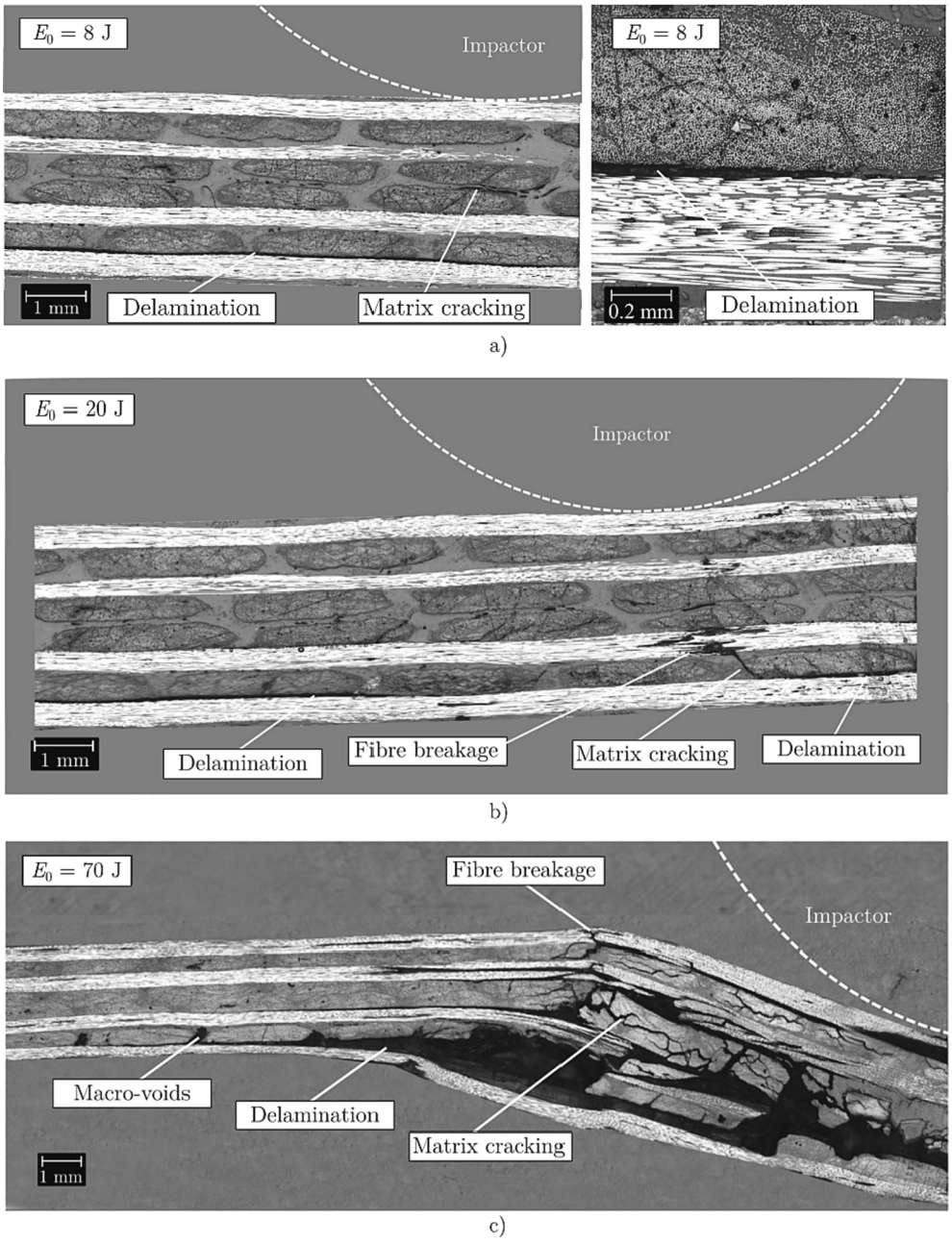

Fig. 10. Different failure mechanism for a) 8 J, b) 20 J, and c) 70 J impacts.

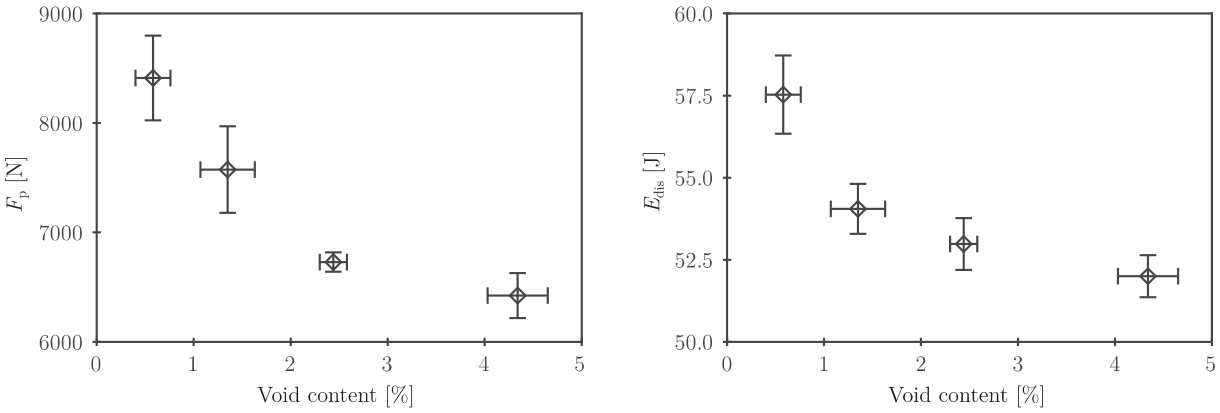

Fig. 11. Reduction of a) peak force, F_p, and b) the dissipated energy, E_{dis}, due to the increase in void content.

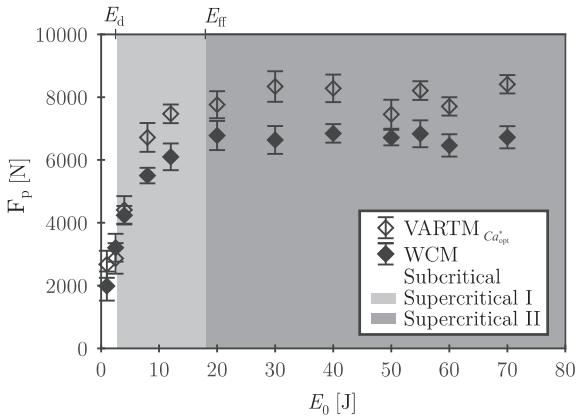

Fig. 12. Ultimate fibre force F_p versus impact energy E_0 for low and high void content plates.

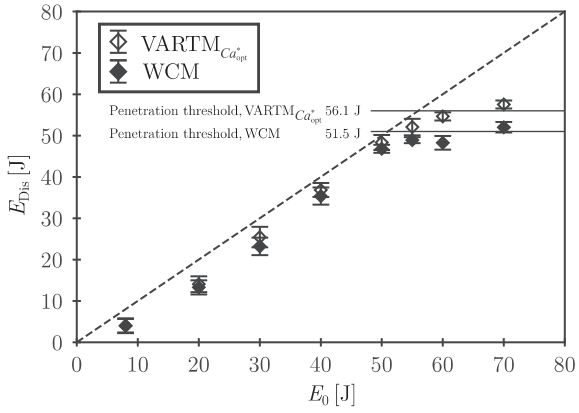

Fig. 13. Dissipated energy E_{dis} versus impact energy E_0 for low and high void content samples.

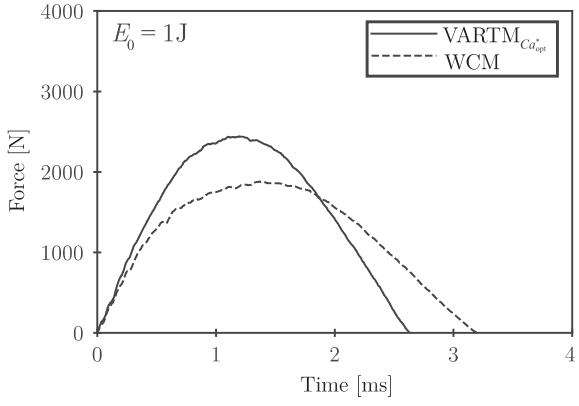

Fig. 14. Force-time curve of subcritical impact (1 J) for low and high void content samples.

then returned to the origin (unload phase, not shown in the figure). The difference in slopes is associated with the difference in bending stiffness [39], with 2100 N/mm and 1365 N/mm corresponding to the stiffness of the samples with low and high void content, respectively. This represents a reduction in stiffness of 35% when comparing the low and high void content plates. Liu et al. [40] obtained similar results, showing a stiffness reduction of 7% for every 1% increase in void content, which would be 28% for 4% void content.

Energies higher than E_d (1.5 J) caused damage to the specimen.

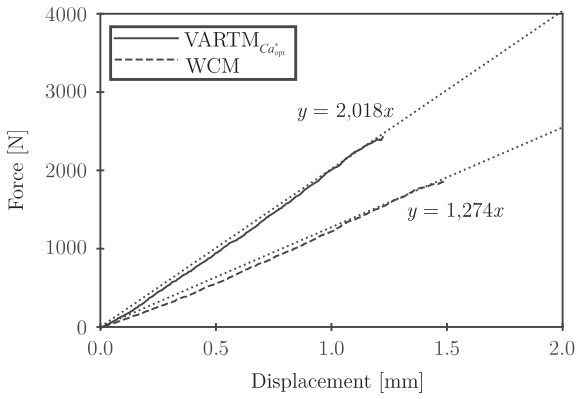

Fig. 15. Force-displacement curve of subcritical impact (1 J) of low and high void content samples.

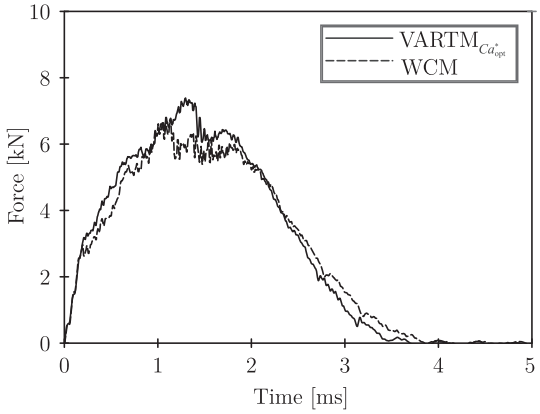

Fig. 16. Force-time curve of supercritical impact (20 J) for low and high void content samples.

Fig. 16 shows the F-t plot of a 20 J impact on the high and low void content specimens. It can be seen that the onset of damage occurs at similar force, around 2500 N, and a reduction in the slope occurs. However, after the onset of damage, the propagation is more severe in the case of the high void content specimens. Several papers in the literature have shown that voids have a detrimental effect on interlaminar shear strength [18,41] and out-of-plane intralaminar shear strength [18,21] for carbon/epoxy NCF laminates manufactured with RTM. Furthermore, Hou et al. [42] demonstrated that the fracture toughness of mode II crack propagation decreases with increasing void content.

This causes fibre breakage to start at a lower energy for a higher void content, thus reaching a lower peak force. In the case of the low void content plate (VARTM$_{opt}$), the peak force was around 7500 N. On the other hand, in the case of the high void content plate (WCM), the force was lower 6700 N. It is worth mentioning that the E_d detected in the 20 J impacts was the same as that previously detected in the 70 J impacts, as it is independent of the incident energy [43].

In terms of the effect of fabric architecture, it can be concluded that the behaviour of NCF fabrics differs somewhat from other 2D architectures. NCF fabrics show similar delamination resistance to woven textiles, which are still inferior to the results obtained with 3D fabrics [39]. In these 3D fabrics, a reinforcement is introduced in the z-direction, and thus, the delamination resistance is increased [44]. However, NCF fabrics, due to their high in-plane performance, allow fibre breakage to occur at higher energy and force. Comparing the results obtained in this work with the results obtained by Zabala et al. with woven textile [45], while in both cases a epoxy resin and 3 mm carbon fibre laminates were used, differences were observed: In both cases both F_d and E_d was

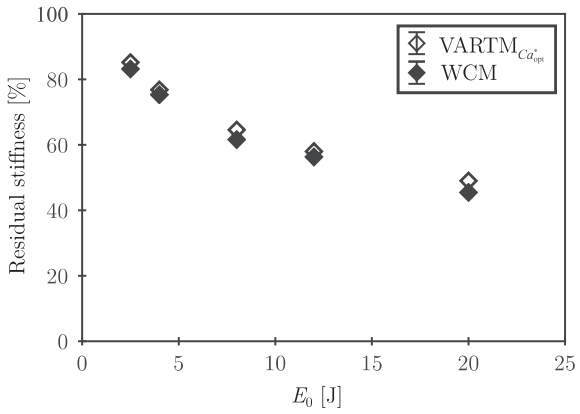

Fig. 17. Residual stiffness evolution curve for low and high void content.

similar, however, both F_p and E_{ff} was higher when using NCF. The NCF material allowed the F_p to increase from 5.9 kN to 8.4 kN, while the E_{ff} increased from 16.5 J to 19.8 J. In another work published by Aurrekoetxea et al. [38] the performance of woven carbon-Epoxy laminate of 3 mm in thickness was studied. They achieved similar E_d value, around 1.5 J similar obtained in the present work. Fibre failure, however, occurred at lower force and energy, 3.8 kN and 30.2 J respectively. This demonstrates the high performance that NCF fabrics can offer on impact.

Furthermore, it is believed that the reduction in impact properties due to porosity is less dependent on the reinforcement and more dependent on the matrix material. This is because matrix-dominated properties are more sensitive than fibre-dominated properties [8]. As several studies have shown, the presence of voids can directly influence the interlaminar behaviour due to the reduction of the cross-sectional area and the stress concentrator effect [46]. However, it is believed that this effect would not be as important in the case of the thermoplastic matrix, as the cracks tend to plasticise [39]. The same explanation was reached by Vieille et al. in their review work where they compared the impact behaviour of thermoplastic and thermoset matrices [47].

3.2.2. Damage tolerance

The effect of impact energy on residual properties was studied by means of the three-test characterisation method. Fig. 17 shows the residual stiffness, which was calculated as the ratio of contact time in subcritical impacts, before and after damaging the specimen. For both cases, the stiffness was reduced up to 50% with impacts of 20 J.

In the 20 J impacts, a slight decrease in the residual stiffness of WCM versus VARTM could be appreciated, being 45.8% and 49.1% residual stiffness respectively. The effect of voids is less noticeable in residual properties than in single impact properties. This may be because once the part is delaminated, the effect of delamination is more pronounced than the effect of void content.

This loss of stiffness is mainly due to the delamination generated in the part. Delamination is one of the main failure modes of fibre-reinforced composites out-of-plane impacts events. It occurs in areas of high interlaminar stress where interlaminar crack initiation and propagation can occur. High interlaminar stress zones usually appear at singular points in the laminate, such as free-edges, internal ply drops and voids [48]. These defects are stress concentrators and usually show the highest interlaminar stresses.

To validate this effect, both samples were analysed by C-scan ultrasonic inspection. Fig. 18 depicts the delaminated region of both specimens impacted with 20 J, which was 16% higher in the WCM specimen (Fig. 18b). It is confirmed, therefore, that the specimen with higher void content suffered higher delamination and therefore the residual stiffness was lower. An increase in defects of this type can result in a reduction of properties and can lead to catastrophic failure in apparently undamaged structures [49].

4. Conclusion

In the present paper, different LCM variants were compared, and their effect on void generation and subsequent impact properties was experimentally quantified.

The WCM process and three variants of RTM were analysed, in which the effect of different injection conditions (application of vacuum and velocity control by capillary number) on void generation was analysed.

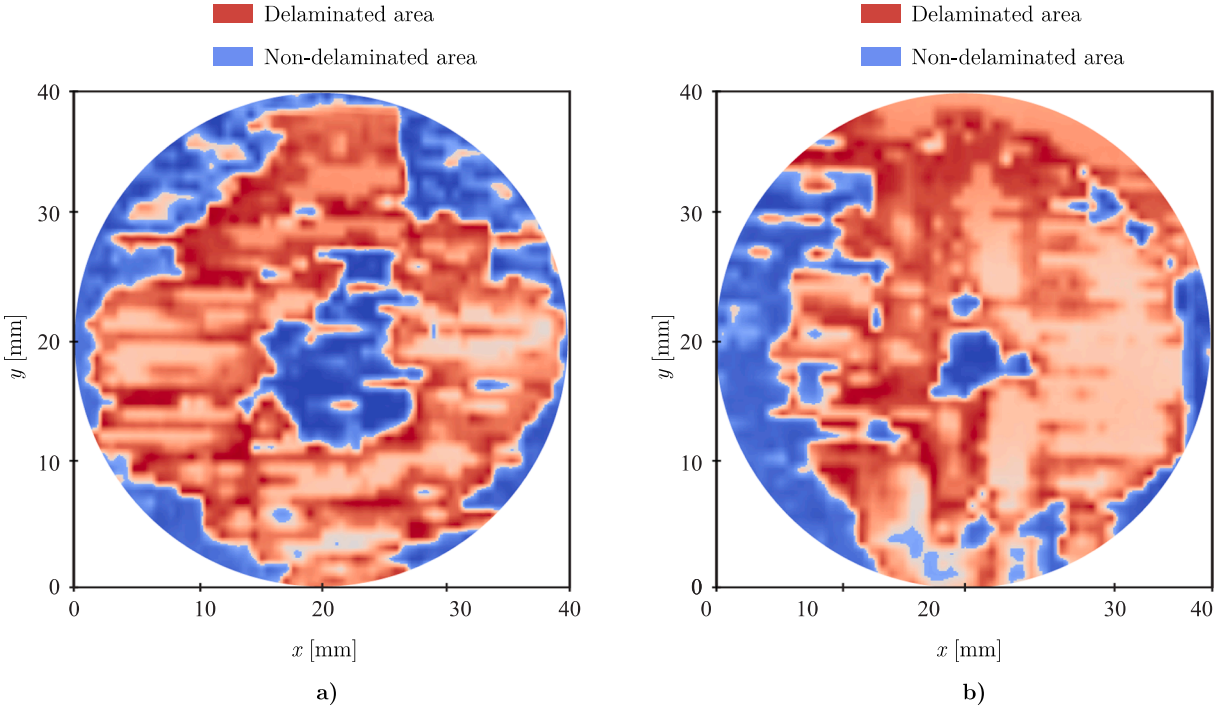

Fig. 18. Delaminated area of a) VARTM sample and b) optimised WCM sample impacted with 20 J.

To obtain the optimum capillary number, the viscosity and surface tension of the resin, and the contact angle between the resin and the fibre were characterised. The process that generated the lowest void content was the VARTM process optimised by capillary number (0.58 ± 0.18%). The RTM process without vacuum application and with velocity control by capillary number generated plates with 1.35 ± 0.28% void content. As regards the third RTM variant, the conventional RTM without vacuum application and velocity optimisation, the void content was 2.44 ± 0.14%. Finally, the WCM process generated the highest void content (4.34 ± 0.31%) as compared to the RTM variants.

The study has been carried out with NCF textile, which has been shown to improve impact properties compared regarding literature woven textiles. Mainly, it has been observed that fibre failure occurs at higher impact energies than woven fabrics. However, the presence of voids has substantially reduced the properties. The increase of void content caused a reduction of 25.88% in ultimate fibre force F_p, and 9.57% in dissipated energy E_{dis}. The perforation and penetration limit was lower in the high void content (WCM) plates; 20% and 30% lower, respectively. In terms of bending stiffness, the low void content plates presented a higher stiffness of 2100 N/mm compared to 1365 N/mm for the high void content plates. Interestingly, the post-impact residual properties were slightly affected by increasing the void content. At high and low voids levels, after an impact of 20 J the specimen retained 45.8% and 49.1% of the stiffness, respectively. The effect of void content is less pronounced on residual properties than on the first impact properties. This may be because once damage is generated in the specimen; the effect of the damage itself is greater than that of the voids.

It is believed that the presence of voids reduces the matrix-dominated properties, which causes the samples to withstand less impact energy. In this work, only the volume of voids has been considered. For future analyses, morphological analysis of the voids is desirable, as this may help to understand better how defects affects the different failure mechanisms.

CRediT authorship contribution statement

Julen Mendikute: Investigation, Writing – original draft, Writing – review & editing. **Maider Baskaran:** Methodology, Supervision. **Laurentzi Aretxabaleta:** Supervision. **Jon Aurrekoetxea:** Methodology, Supervision.

Declaration of Competing Interest

The authors declare that they have no known competing financial interests or personal relationships that could have appeared to influence the work reported in this paper.

Acknowledgement

The authors acknowledge the valuable help of Dr. Jaime Castro and Dr. Carlos Gonzalez during the characterisation of the contact angle and surface tension of the resin carried out at IMDEA Materials. J. Mendikute thanks the Basque Government for the predoctoral training grant (PRE_2018_1_0338). Authors would also like to thank the Basque Government for providing financial support (IT833-16; KK-2017/00062) for this study.

References

[1] González C, Vilatela JJ, Molina-Aldareguía JM, Lopes CS, LLorca J. Structural composites for multifunctional applications: Current challenges and future trends. Prog Mater Sci 2017;89:194–251. doi:10.1016/j.pmatsci.2017.04.005.
[2] Richardson MOW, Wisheart MJ. Review of low-velocity impact properties of composite materials. Compos Part A Appl Sci Manuf 1996;27:1123–31. https://doi.org/10.1016/1359-835X(96)00074-7.
[3] Wisnom MR. The role of delamination in failure of fibre-reinforced composites. The role of delamination in failure of fibre-reinforced composites 2012;370(1965):1850–70.
[4] Lomov SV, Truong Chi T, Verpoest I. Mechanical properties of non-crimp fabric (NCF) based composites: stiffness and strength. Non-Crimp Fabr Compos, Woodhead Publishing Limited 2011:263–88. https://doi.org/10.1533/9780857092533.3.263.
[5] Bel S. Mechanical behaviour of non-crimp fabric (NCF) preforms in composite materials manufacturing. Adv Compos Manuf Process Des, Elsevier Ltd 2015:253–68. https://doi.org/10.1016/B978-1-78242-307-2.00012-9.
[6] Henning F, Kärger L, Dörr D, Schirmaier FJ, Seuffert J, Bernath A. Fast processing and continuous simulation of automotive structural composite components. Compos Sci Technol 2019;171:261–79. https://doi.org/10.1016/j.compscitech.2018.12.007.
[7] Mesogitis TS, Skordos AA, Long AC. Uncertainty in the manufacturing of fibrous thermosetting composites: A review. Compos Part A Appl Sci Manuf 2014;57:67–75. https://doi.org/10.1016/j.compositesa.2013.11.004.
[8] Liu C. A review of void formation and its effects on the mechanical performance of carbon fiber reinforced plastic. Eng Trans 2016;64:33–51.
[9] Hamidi YK, Altan CM. 25 Process-Induced Defects in Resin Transfer Molded Composites 2018;vol. 2. https://doi.org/10.1016/b978-0-12-803581-8.09902-1.
[10] Bodaghi M, Cristóvão C, Gomes R, Correia NC. Experimental characterization of voids in high fibre volume fraction composites processed by high injection pressure RTM. Compos Part A Appl Sci Manuf 2016;82:88–99. https://doi.org/10.1016/j.compositesa.2015.11.042.
[11] Patel N, Rohatgi V, Lee LJ. Micro scale flow behavior and void formation mechanism during impregnation through a unidirectional stitched fiberglass mat. Polym Eng Sci 1995;35(10):837–51.
[12] Trochu F, Ruiz E, Achim V, Soukane S. Advanced numerical simulation of liquid composite molding for process analysis and optimization. Compos Part A Appl Sci Manuf 2006;37:890–902. https://doi.org/10.1016/j.compositesa.2005.06.003.
[13] Ruiz E, Achim V, Soukane S, Trochu F, Bréard J. Optimization of injection flow rate to minimize micro/macro-voids formation in resin transfer molded composites. Compos Sci Technol 2006;66:475–86. https://doi.org/10.1016/j.compscitech.2005.06.013.
[14] Ravey C, Ruiz E, Trochu F. Determination of the optimal impregnation velocity in Resin Transfer Molding by capillary rise experiments and infrared thermography. Compos Sci Technol 2014;99:96–102. https://doi.org/10.1016/j.compscitech.2014.05.019.
[15] Mehdikhani M, Gorbatikh L, Verpoest I, Lomov SV. Voids in fiber-reinforced polymer composites: A review on their formation, characteristics, and effects on mechanical performance. J Compos Mater 2019;53:1579–669. https://doi.org/10.1177/0021998318772152.
[16] Kosmann N, Karsten JM, Schuett M, Schulte K, Fiedler B. Determining the effect of voids in GFRP on the damage behaviour under compression loading using acoustic emission. Compos Part B Eng 2015;70:184–8. https://doi.org/10.1016/j.compositesb.2014.11.010.
[17] Montoro SR, Shiino MY, Da Cruz TG, Cioffi MOH, Woorwald HJC. Influence of voids on the flexural resistance of the NCF/RTM6 composites. Procedia Eng 2011;10:3220–5. https://doi.org/10.1016/j.proeng.2011.04.532.
[18] Sisodia S, Gamstedt EK, Edgren F, Varna J. Effects of voids on quasi-static and tension fatigue behaviour of carbon-fibre composite laminates. J Compos Mater 2015;49:2137–48. https://doi.org/10.1177/0021998314541993.
[19] Gehrig F, Mannov E, Schulte K. Degradation of NCF-epoxy composites containing voids. ICCM Int Conf Compos Mater 2009.
[20] Protz R, Kosmann N, Gude M, Hufenbach W, Schulte K, Fiedler B. Voids and their effect on the strain rate dependent material properties and fatigue behaviour of non-crimp fabric composites materials. Compos Part B Eng 2015;83:346–51.
[21] Carraro PA, Maragoni L, Quaresimin M. Influence of manufacturing induced defects on damage initiation and propagation in carbon/epoxy NCF laminates. Adv Manuf Polym Compos Sci 2015;1:44–53. https://doi.org/10.1179/2055035914Y.0000000004.
[22] Huang H, Talreja R. Effects of void geometry on elastic properties of unidirectional fiber reinforced composites. Compos Sci Technol 2005;65(13):1964–81.
[23] Kakakasery J, Arumugam V, Abdul Rauf K, Bull D, Chambers AR, Scarponi C, et al. Cure cycle effect on impact resistance under elevated temperatures in carbon prepreg laminates investigated using acoustic emission. Compos Part B Eng 2015;75:298–306.
[24] Kousourakis A, Mouritz AP, Bannister MK. Interlaminar properties of polymer laminates containing internal sensor cavities. Compos Struct 2006;75(1-4):610–8.
[25] Arthurs B, Bull DJ, Arumugam V, Chambers AR, Santulli C. Porosity effect on residual flexural strength following low energy impact of carbon fibre composites. Polym Polym Compos 2015;23(4):205–12.
[26] Leclerc JS, Ruiz E. Porosity reduction using optimized flow velocity in Resin Transfer Molding. Compos Part A Appl Sci Manuf 2008;39(12):1859–68.
[27] Estrada G, Vieux-Pernon C, Advani SG. Experimental characterization of the influence of tackifier material on preform permeability. J Compos Mater 2002;36:2297–310. https://doi.org/10.1177/0021998302036019542.
[28] Bodaghi M, Costa R, Gomes R, Silva J, Correia N, Silva F. Experimental comparative study of the variants of high-temperature vacuum-assisted resin transfer moulding. Compos Part A Appl Sci Manuf 2019;129:105708. https://doi.org/10.1016/j.compositesa.2019.105708.
[29] Wilhelmy L. Ueber die Abhängigkeit der Capillaritäts-Constanten des Alkohols von Substanz und Gestalt des benetzten festen Körpers. Ann Phys 1863;195(6):177–217.
[30] Castro J, Sket F, González C. S-XCT experimental determination of local contact angle and meniscus shape in liquid moulding of composites. Compos Sci Technol 2020;199:108362. https://doi.org/10.1016/j.compscitech.2020.108362.

[31] Lystrup C, George A, Zobell B, Boster K, Childs C, Girod H, et al. Optical measurement of voids in situ during infusion of carbon reinforcements. J Compos Mater 2021;55(6):775–86.
[32] Lee S, Hong C, Choi T, Kim H-G, Im S-W, Kang S-C, et al. CSAI analysis of non-crimp fabric cross-ply laminate manufactured through wet compression molding process. Compos Struct 2021;255:113056.
[33] Feraboli P, Kedward KT. Enhanced evaluation of the low-velocity impact response of composite plates. AIAA J 2004;42:2143–52. https://doi.org/10.2514/1.4534.
[34] Feraboli P, Kedward KT. A new composite structure impact performance assessment program. Compos Sci Technol 2006;66:1336–47. https://doi.org/10.1016/j.compscitech.2005.09.009.
[35] Bodaghi M, Simacek P, Correia N, Advani SG. Experimental parametric study of flow-induced fiber washout during high-injection-pressure resin transfer molding. Polym Compos 2020;41(3):1053–65.
[36] Lebel F, Ruiz E, Trochu F. Void content analysis and processing issues to minimize defects in liquid composite molding. Polym Compos 2017;40:109–20. https://doi.org/10.1002/pc.24609.
[37] Zabala H, Aretxabaleta L, Castillo G, Urien J, Aurrekoetxea J. Impact velocity effect on the delamination of woven carbon-epoxy plates subjected to low-velocity equienergetic impact loads. Compos Sci Technol 2014;94:48–53. https://doi.org/10.1016/j.compscitech.2014.01.016.
[38] Aurrekoetxea J, Agirregomezkorta A, Aretxaga G, Sarrionandia M. Impact behavior of carbon fiber/epoxy composite manufactured by vacuum-assisted compression resin transfer molding. J Compos Mater 2012;46:43–9. https://doi.org/10.1177/0021998311401938.
[39] Shah SZH, Karuppanan S, Megat-Yusoff PSM, Sajid Z. Impact resistance and damage tolerance of fiber reinforced composites: A review. Compos Struct 2019;217:100–21. https://doi.org/10.1016/j.compstruct.2019.03.021.
[40] Liu L, Zhang B-M, Wang D-F, Wu Z-J. Effects of cure cycles on void content and mechanical properties of composite laminates. Compos Struct 2006;73(3):303–9.
[41] Varna J, Joffe R, Berglund LA, Lundström TS. Effect of voids on failure mechanisms in RTM laminates. Compos Sci Technol 1995;53(2):241–9.
[42] Hou M, Ye L, Mai Y-W. Effect of moulding temperature on flexure, impact strength and interlaminar fracture toughness of CF/PEI composite. J Reinf Plast Compos 1996;15(11):1117–30.
[43] Cartié DDR, Irving PE. Effect of resin and fibre properties on impact and compression after impact performance of CFRP. Compos - Part A Appl Sci Manuf 2002;33(4):483–93.
[44] Mouritz AP. Ballistic impact and explosive blast resistance of stitched composites. Compos Part BEngineering 2001;32(5):431–9.
[45] Zabala H. Influencia de la velocidad de impacto en la delaminación generada por impactos transversales de baja velocidad en tejidos carbono- epoxi. Dependencia del comportamiento interlaminar del composite a la velocidad de propagación de grieta. Mondragon Unibertsitatea; 2014.
[46] Tretiak I, Kawashita LF, Hallett SR. Predicting short beam shear strength reduction in carbon/epoxy laminates containing voids. Compos Struct 2022;290:115472. https://doi.org/10.1016/j.compstruct.2022.115472.
[47] Vieille B, Casado VM, Bouvet C. About the impact behavior of woven-ply carbon fiber-reinforced thermoplastic- and thermosetting-composites: A comparative study. Compos Struct 2013;101:9–21.
[48] Turon A, Camanho PP, Soto A, González EV. Analysis of delamination damage in composite structures using cohesive elements. Compr Compos Mater II 2017. https://doi.org/10.1016/B978-0-12-803581-8.10059-1.
[49] David-West OS, Nash DH, Banks WM. An experimental study of damage accumulation in balanced CFRP laminates due to repeated impact. Compos Struct 2008;83:247–58. https://doi.org/10.1016/j.compstruct.2007.04.015.